

Article

Illustration of Convective Boundary Conditions on the Darcy–Forchheimer Flow of Nanofluid with the Impact of Chemical Reaction

Priyashree Chandini Pattanaik ^{1,†}, Swarnalata Jena ¹, Satya Ranjan Mishra ^{2,*}, Mansoor Alshehri ³ 
and Nehad Ali Shah ^{4,*}, [†]

- ¹ Department of Mathematics, Centurion University of Technology and Management, Bhubaneswar 752050, India; 190506152001@cutm.ac.in (P.C.P.); swarnalata.jena@cutm.ac.in (S.J.)
² Department of Mathematics, Siksha ‘O’ Anusandhan Deemed to be University, Khandagiri, Bhubaneswar 751030, India
³ Department of Mathematics, College of Sciences, King Saud University, P.O. Box 2455, Riyadh 11451, Saudi Arabia; mhalshehri@ksu.edu.sa
⁴ Department of Mechanical Engineering, Sejong University, Seoul 05006, Republic of Korea
* Correspondence: satyaranjanmishra@soa.ac.in (S.R.M.); nehadali199@sejong.ac.kr (N.A.S.)
[†] These authors contributed equally to this work and are co-first authors.

Abstract: The application of convective heat transport holds great significance in physiological studies, particularly in preventing the overheating of birds and mammals living in warm climates. This process involves the transfer of heated blood from the body’s core to the nearest blood vessels, effectively dissipating the excess heat into the environment. As a result, analyzing convective boundary conditions becomes crucial for understanding heat and solutal profiles in the flow of a two-phase nanofluid model (Darcy–Forchheimer), which also takes into account heat sources and chemical reactions. This model encompasses the combined effects of Brownian and thermophoresis phenomena on flow behavior. The development of a three-dimensional model leads to a set of nonlinear ODEs, which can be tackled using appropriate similarity variables and traditional numerical techniques, i.e., the Runge–Kutta fourth-order combined with shooting technique is adopted to obtain the solutions. To ensure the model’s accuracy, physical parameters are carefully chosen within their appropriate ranges to reflect real-world behavior. This approach helps to capture the physical essence of the system under study. It is observed that the streamlines for the proposed stream function shows the flow pattern of the fluid particles within the domain for the variation of the kinematic viscosity and stream values, and enhanced Brownian motion controls the fluid concentration.

Keywords: nanofluid; Darcy–Forchheimer model; Brownian and thermophoresis; chemical reaction; convective boundary conditions; numerical method



Citation: Pattanaik, P.C.; Jena, S.; Mishra, S.R.; Alshehri, M.; Shah, N.A. Illustration of Convective Boundary Conditions on the Darcy–Forchheimer Flow of Nanofluid with the Impact of Chemical Reaction. *Symmetry* **2023**, *15*, 1728. <https://doi.org/10.3390/sym15091728>

Academic Editors: Dário Ferreira and Calogero Vetro

Received: 30 July 2023

Revised: 31 August 2023

Accepted: 6 September 2023

Published: 8 September 2023



Copyright: © 2023 by the authors. Licensee MDPI, Basel, Switzerland. This article is an open access article distributed under the terms and conditions of the Creative Commons Attribution (CC BY) license (<https://creativecommons.org/licenses/by/4.0/>).

1. Introduction

Research into nanofluids is currently experiencing growth due to the limitations of thermal properties found in conventional base fluids. Among the various physical attributes, thermal conductivity emerges as a pivotal factor owing to its significance. Common base liquids such as ethyl alcohol, water, kerosene, and ethylene glycol exhibit notably lower thermal efficiency compared to nanoparticles. Consequently, augmenting these base liquids (coolants) with nano-sized particles of metals, oxides, or carbides, known as “nanofluids,” can elevate their thermal performance. Nanofluids bring about significant alterations in density, viscosity, diffusivity, and thermal conductivity compared to conventional fluids. These nanofluids hold immense promise in addressing heat management challenges, thereby expanding the horizons for nanomaterial applications across various industries. Notable applications include thermal energy transportation, heat exchangers, thermal power plants, microelectronics, automobile cooling, physiological contexts such as

peristaltic pumping, drug delivery processes, medical instruments, and solar panels for electricity generation.

After conducting a series of experiments on nanofluids, Choi [1] and Choi et al. [2] significantly contributed to the goal of enhancing the efficiency of heat transfer fluids. This research endeavor has been further advanced by numerous scholars [3–6]. The application of stretching flows spans a wide array of sectors, including aerodynamics, industrial simulations, chemical processing, electronic device cooling, centrifugal filtration techniques, and Burke–Schumann flames. Crane [7] extensively investigated flow over an expanding cylinder, while Fang and Yao [8] conducted a dependable experiment concerning the flow past a stretching cylinder in viscous fluid. In a parallel channel embedded within a permeable medium, Pattanaik and colleagues [9] examined the effects of buoyancy on the “Williamson nanofluid” flow. Their study utilized the “Adomian Decomposition Method”, a semi-analytical approach, to solve the relevant equations. The findings indicated that an increased particle concentration led to a noteworthy elevation in fluid temperature compared to the pure fluid, albeit with a decrease in fluid velocity. The volume fraction of particles also exerted a significant influence on enhancing fluid temperature. In another context, Naseer et al. [10] presented an experimental overview of fluid flow through an expanding cylinder, revealing an exponential expansion with surface thickness. Ma-jeed et al. [11] conducted a meaningful analysis of partial slip effects on heat transfer in the context of an expanding cylinder, delving into the intricacies of thermal transport phenomena.

Considering the combined effects of cross-diffusion and radiation, Hosseinzadeh et al. [12] provided a more comprehensive understanding of second-grade fluid behavior in the context of a stretching cylinder. In the application towards enhancing the heat transfer rate, the role of MHD combined with thermal radiation plays a vital role. Therefore, it is currently the keen interest of several researchers. Recent applications include electric power generation, the cooling of electronic devices, the cooling of underground electric cables, controlling the temperature at production processes, geophysics, and the cooling of nuclear reactors, vis-à-vis the blood flow through arteries in the human body, plasma studies, etc. However, these behaviors can be studied by the consideration of the well-posed Navier–Stokes equations in association with the Maxwell equations. Zhou et al. [13] proposed their investigation on nanofluid for the impact of particle concentration and electromagnetic field within an enclosure. They also concluded that the heat transfer rate varies with enhanced particle concentration and is affected in opposite directions by the inclusion of a magnetic field. Ashorynejad et al. [14] considered the nanofluid flow contributing to the improvement process of transport phenomena over an elongating cylinder. To ensure a more effective flow, Mukhopadhyay [15] put thrust on the MHD flow properties of nanofluid conspiring within a thermally-stratified region. Based on an assessment of the consequences of MHD, Tlili [16] aimed at considering Jeffrey fluid for the inclusion of heat generation under the surrounding microgravity. Javaherdeh et al. [17] studied the role of cross-diffusion on MHD flow within a permeable medium for a vertical sliding plate using FDM, resulting that the fluid temperature augments with enhanced magnetic parameter and the impact is the opposite for the porosity parameter. Raju et al. [18] analyzed different parameter effects associated with MHD stretching sheets for both Newtonian and non-Newtonian nanofluid. They concluded that the augmentation in the volume fraction enhanced the heat transfer rate, whereas the magnetic field increased the shear rate, which makes the fluid temperature lower, and the heat source/sink parameter enhanced the fluid temperature. Sheikholeslami [19,20] investigated the magnetic field effect in nanofluid using the mesoscopic method where CuO was taken as the nanoparticle and water was the base fluid with concentrations from 0 to 0.04. Sheikholeslami found that the Hartmann number augments heat transfer and Lorentz’s force reduces the velocity of nanofluid which helps in increasing thermal bounding surface thickness. Wakif et al. [21] investigated nanofluid convection for the occurrence of an applied magnetic field on the basis of the non-homogeneous Buongiorno’s model by using analytical techniques. However, the

behavior of several physical belongings of some conducting nanofluids in a two-phase transport model is described briefly. Bhatti et al. [22] proposed a 3D unsteady MHD flow of viscous nanofluid, by taking a stretching porous cylinder having gyrotactic microorganisms, which was numerically solved by employing a shooting technique associated with non-linear thermal radiation and reacting species. Slip effects are also considered, and it was concluded that fluid velocity retards for the inclusion of a magnetic field and porosity. Further, radiation amplifies the fluid temperature, whereas a thermal slip parameter shows opposite effect.

The study of nanofluid in the porous medium gives detail by enabling the transport of heat and fluid velocity which is used in several applications in the fields of agriculture, engineering, and industries [23]. Darcy's law generally aims to show the properties of the flow of this medium, yet in the case of higher velocity it is imperial to utilize the extended Darcy–Forchheimer model. The Darcy model is basically a comprehensive substantial form of Darcian flow usually implanted for inertia effects. On adding the outcome of inertia with presumed square word to the velocity expression, the Forchheimer's modified is derived. Hayat et al. [24] published an important study on Williamson nanofluid under a convective surface condition in a 3D Darcy–Forchheimer model. Muhammad et al. [25] extensively studied zero nanoparticle mass flux and thermal convective conditions and subsequently analyzed the flow of nanofluid considering the similar Darcy–Forchheimer model. Jena et al. [26–28] numerically analyzed the behavior of nanomaterials for some special types of nanofluid. Adequate research was conducted by Hayat et al. [29] and they have proposed Xue model thermal conductivity with carbon nanotubes (CNT) as the nanoparticles.

A significant experiment was conducted by Ramesh [30] between three-dimensional Darcy–Forchheimer inertial drag in Casson nanofluid for the presence of a heating device; the details resolve about the Casson parameter responsible for heat augmentation. Muskat [31] represented the new concept as attributed to Forchheimer. Muhammad et al. [32] executed a fundamental study to show the flow of a hybrid nanofluid using inertial drag all through a permeable rotating disk. Rasool et al. [33] used a confined non-linearly stretched surface to derive the numerical value of the drag presented in the flow of MHD nanofluid. A complete detailed summary of entropy generation (EG) was given by Nayak et al. [34] by non-linearly manipulating the flow of SWCNT/MWCNT as nanoparticles. The research work majorly reveals the significant characteristics of hybrid nanofluids and helps to understand it in terms of the various properties of flow phenomena. Atashafrooz et al. [35] presented the combined convective–radiative heat transfer of hybrid nanofluid flow within an open trapezoidal enclosure. The research delves into the influence of magnetic forces on the heat transfer process. Their findings offer insights into enhancing heat transfer efficiency in innovative enclosure geometries. Further, the study by Atashafrooz et al. [36] investigates the characteristics of nanofluid flow within a trapezoidal recess. By considering the interplay of the Lorentz force and bleeding effects, the research delves into complex heat and mass transfer behaviors. Incorporating thermodynamical analysis, the paper sheds light on fundamental insights into nanofluid behavior [37,38].

Based upon the literature mentioned earlier, this current investigation aims to explore the influence of convective boundary conditions on the flow of a two-phase nanofluid over an expanding surface that is embedded within a porous matrix. The inclusion of factors such as Darcy–Forchheimer inertial drag, heat source, and chemical reaction significantly enhances the complexity of the flow phenomena. To solve the modified non-dimensional governing equations, a numerical approach, specifically the Runge–Kutta–Fehlberg method, is employed. A comparative analysis with a previous study demonstrates strong agreement in a specific scenario.

2. Formulation of the Model

A three-dimensional Darcy–Forchheimer model considering two-phase nanofluid flow via an elongating surface through a permeable medium is proposed in this article. The flow is supposed to move in both directions of the stretching sheet, imposing the

cross-diffusion effects. Additionally, the effect of a chemical reaction with the convective heat transfer and zero nanoparticles flux are introduced at the boundary which enriches the profile. The configuration of the system is arranged such that the x - and y -axes align with the surface's stretching direction, while the z -axis is perpendicular to it. The velocities corresponding to the stretching direction are denoted as $u_w = ax$ along the x -axis and $v_w = by$ along the y -axis. The convective heat process suggests the transport coefficient as h_f and T_f considered as the surface temperature with hot fluid (Figure 1). Following Muhammad et al. [25], the modelling of the physical problem is described as

$$\frac{\partial u}{\partial x} + \frac{\partial v}{\partial y} + \frac{\partial w}{\partial z} = 0 \quad (1)$$

$$u \frac{\partial u}{\partial x} + v \frac{\partial u}{\partial y} + w \frac{\partial u}{\partial z} = v \frac{\partial^2 u}{\partial z^2} - \frac{v}{K} u - Fu^2 - \frac{\sigma B_0^2 u}{\rho} \quad (2)$$

$$u \frac{\partial v}{\partial x} + v \frac{\partial v}{\partial y} + w \frac{\partial v}{\partial z} = v \frac{\partial^2 v}{\partial z^2} - \frac{v}{K} v - Fv^2 - \frac{\sigma B_0^2 v}{\rho} \quad (3)$$

$$u \frac{\partial T}{\partial x} + v \frac{\partial T}{\partial y} + w \frac{\partial T}{\partial z} = \alpha_m \frac{\partial^2 T}{\partial z^2} + \frac{(\rho c)_p}{(\rho c)_f} \left(D_B \left(\frac{\partial T}{\partial z} \frac{\partial C}{\partial z} \right) + \frac{D_T}{T_\infty} \left(\frac{\partial T}{\partial z} \right)^2 \right) + \frac{Q_0}{(\rho c)_f} (T - T_\infty) \quad (4)$$

$$u \frac{\partial C}{\partial x} + v \frac{\partial C}{\partial y} + w \frac{\partial C}{\partial z} = D_B \left(\frac{\partial^2 C}{\partial z^2} \right) + \frac{D_T}{T_\infty} \left(\frac{\partial^2 T}{\partial z^2} \right) - kc^*(C - C_\infty) \quad (5)$$

with the surface conditions

$$\left. \begin{aligned} u = ax, v = by, w = 0, -k \frac{\partial T}{\partial z} = h_f (T_f - T), D_B \frac{\partial C}{\partial z} + \frac{D_T}{T_\infty} \frac{\partial T}{\partial z} = 0, \text{ at } z = 0 \\ u \rightarrow 0, v \rightarrow 0, T \rightarrow T_\infty, C \rightarrow C_\infty \quad \text{as } z \rightarrow \infty \end{aligned} \right\} \quad (6)$$

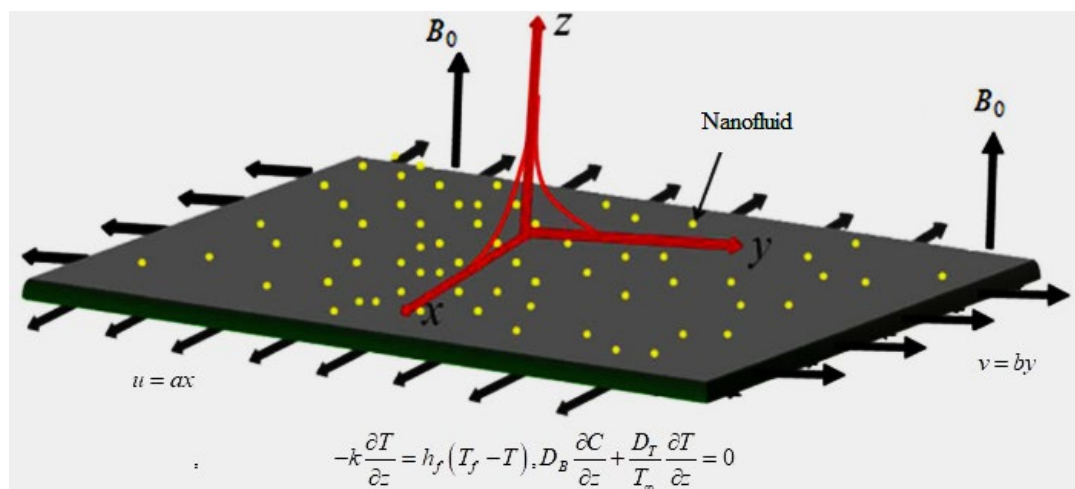


Figure 1. Flow configuration.

Here, (u, v, w) indicates the momentum components towards (x, y, z) directions correspondingly; $\nu \left(= \frac{\mu}{\rho_f} \right)$, kinematic viscosity; ρ_f , density; μ , dynamic viscosity; K , permeability; $F \left(= \frac{C_b}{xK^2} \right)$, drag coefficient; C_b , the amount of drag; T , fluid temperature; and $\alpha_m \left(= \frac{k}{(\rho c)_f} \right)$, thermal diffusivity, where k represents conductivity; $(\rho c)_p$, $(\rho c)_f$, heat capacity of solid and the base fluid, respectively; C , concentration; D_B , D_T are the Brownian and thermophoretic diffusion; T_∞ , C_∞ are denoted as temperature and concentration for the ambient state; and a and b are constants.

The proposed similarity variables are

$$\begin{aligned} u &= axf'(\zeta), v = ayg'(\zeta), w = -(av)^{1/2}(f + g), \\ \theta(\zeta) &= \frac{T - T_\infty}{T_w - T_\infty}, \phi(\zeta) = \frac{C - C_\infty}{C_\infty}, \zeta = \left(\frac{a}{v}\right)^{1/2} z \end{aligned} \quad (7)$$

Substitution of (7) satisfies Equation (1) whereas Equations (2)–(6) lead to

$$f''' + (f + g)f'' - f'^2 - \lambda f' - Frf'^2 - Mf' = 0 \quad (8)$$

$$g''' + (f + g)g'' - g'^2 - \lambda g' - Frg'^2 - Mg' = 0 \quad (9)$$

$$\theta'' + Pr((f + g)\theta' + Nb\theta'\phi' + Nt\theta'^2 + S\theta) = 0 \quad (10)$$

$$\phi'' + LePr(f + g)\phi' + \frac{Nt}{Nb}\theta'' - LePrKc\phi = 0 \quad (11)$$

$$\left. \begin{aligned} f(0) &= g(0) = 0, f'(0) = 1, g'(0) = \alpha, \\ \theta'(0) &= -\gamma(1 - \theta(0)), Nb\phi'(0) + Nt\theta'(0) = 0, \\ f'(\infty) &\rightarrow 0, g'(\infty) \rightarrow 0, \theta(\infty) \rightarrow 0, \phi(\infty) \rightarrow 0 \end{aligned} \right\} \quad (12)$$

where λ , porosity matrix; Fr , inertial drag; α , velocity ratio; Pr , Prandtl number; Sc , usually stands for Schmidt number; γ , indicates Biot number; Nt , thermophoresis; and Nb , Brownian motion.

However, the description of the parameters are

$$\left. \begin{aligned} \lambda &= \frac{v}{ka}, Fr = \frac{C_b}{K^{1/2}}, \alpha = \frac{b}{a}, Pr = \frac{v}{\alpha_m}, Sc = \frac{v}{D_B}, \\ \gamma &= \frac{h_f}{k} \sqrt{\frac{v}{a}}, Nt = \frac{(\rho c)_p D_T (T_f - T_\infty)}{(\rho c)_f v T_\infty}, Nb = \frac{(\rho c)_p D_B (C_\infty)}{(\rho c)_f v} \\ Kc &= \frac{kc^*}{a}, S = \frac{Q_0}{(\rho c)_p a}, M = \frac{\sigma B_0^2}{\rho a} \end{aligned} \right\} \quad (13)$$

Dimensionless relations of skin-friction coefficients, local Nusselt, and Sherwood numbers are as follows:

$$\left. \begin{aligned} Re_x^{1/2} C_{fx} &= -f''(0), \\ Re_y^{1/2} C_{fy} &= -\alpha^{-3/2} g''(0), \\ Re_x^{-1/2} Nu_x &= -\theta'(0) \end{aligned} \right\} \quad (14)$$

Here, the local Reynolds numbers are $Re_x = U_W x / v$ and $Re_y = V_W y / v$.

3. Discussion on the Present Outcomes

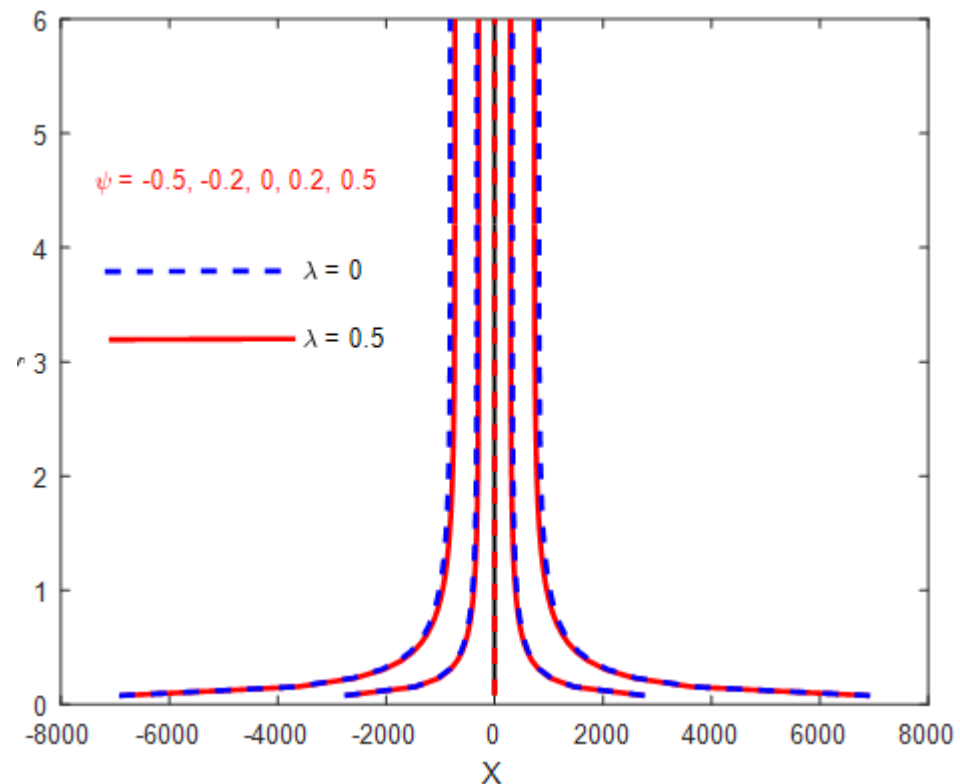
The assumption of two-phase nanofluid over the bidirectional movement of the stretching surface imposed with a porous matrix is deployed here. The electrically conducting fluid with a collaboration of ‘‘Darcy–Forchheimer’’ model inertial drag, additional heat source, and reacting species enriches the flow phenomena significantly. The proposed designed model is taken care of by the Runge–Kutta–Fehlberg technique and, further, the parametric behavior is exhibited for their appropriate values within the particular range. The validation vis-à-vis the conformity of the convergence criteria with the earlier investigated results in particular cases is displayed in Table 1. It reveals from Table 1 that the present outcome shows a good correlation with Muhammad et al. [25] for several values of the parameters presented thereat. The computational results of the error indicate the accuracy of the present methodology with that of the earlier methodology and provide strength to precede our investigation in this direction. The computational behavior of the various constraints is presented through Figures 2–16 for the fixed values of the following $M = 0.5$; $\lambda = 0.2$; $Fr = 1$; $Pr = 6.2$; $Nt = 0.2$; $Nb = 0.5$; $S = -0.2$; $Le = 1$; $\alpha = 0.1$; $Kc = 0.1$; $\gamma = 0.1$; and further the variation of the specific limitation is reflected separately in each figure.

Table 1. Validation of C_f for λ , Fr , and α .

λ	Fr	α	Muhammad et al. [25]	Present	%Error	Muhammad et al. [25]	Present	%Error
0	0.1	0.2	−1.06945	−1.069721153	0.02535	−1.67684	−1.6783698	0.0912
0.1			−1.11471	−1.114869506	0.01430	−1.81669	−1.8175236	0.0458
0.2			−1.1583	−1.158393095	0.00803	−1.94722	−1.9476868	0.0239
	0		−1.13041	−1.130505087	0.00841	−1.93414	−1.934598	0.0236
	0.1		−1.1583	−1.158393095	0.00803	−1.94722	−1.9476868	0.0239
	0.2		−1.18561	−1.18570202	0.00776	−1.96037	−1.9608405	0.0240
	0.1	0.1	−1.1416	−1.14171863	0.01039	−2.54234	−2.5433014	0.0378
		0.3	−1.17449	−1.174565295	0.00641	−1.70234	−1.7026137	0.0160
		0.5	−1.20563	−1.205688659	0.00486	−1.47621	−1.4763267	0.0079

3.1. Streamlines (Flow Pattern)

Figures 2 and 3 show the plots for the streamlines due to the use of stream function and the kinematic viscosity in the considerable c of the porous matrix, respectively. These plots represent the flow pattern of each particle within the domain. In particular, the difference between the values of stream function at any two points declares the volumetric rates through a line. It also indicates the tangent to the flow velocity where the values of the stream function should be constant along a streamline. An interesting observation is that with the variation of the stream function and the kinematic viscosity, the intensity of the nanofluid enhances on the stretching surface with a stagnation point marked at $X = 0$. Further, the sharpness observed towards the free stream increases from the stagnation point. The flow through a permeable medium also shows a greater deceleration and therefore the amount of sharpness increases significantly.

**Figure 2.** Streamlines for the variation of ψ .

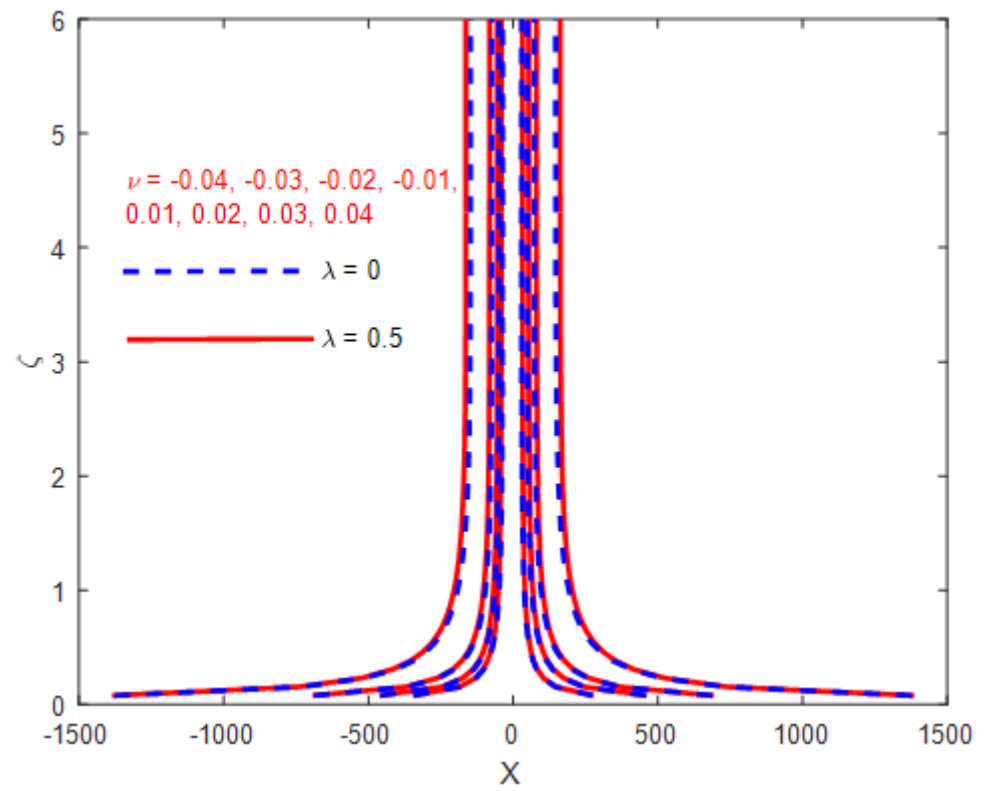


Figure 3. Streamlines for various kinematic viscosities.

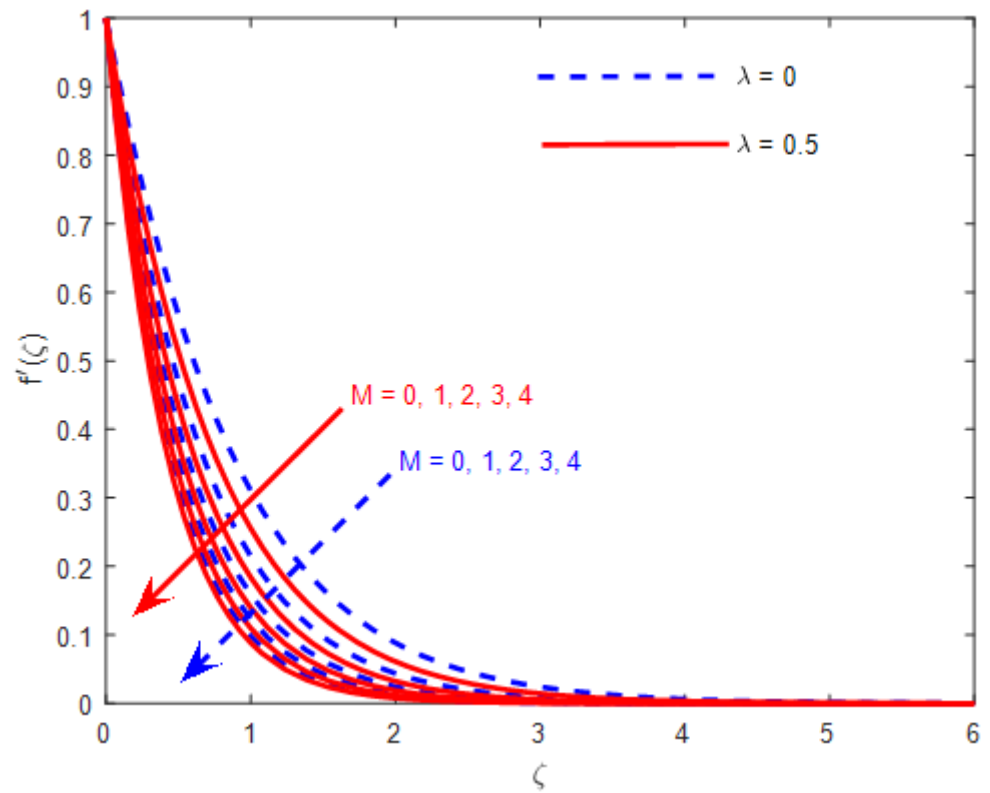


Figure 4. Variation of M and λ on axial velocity.

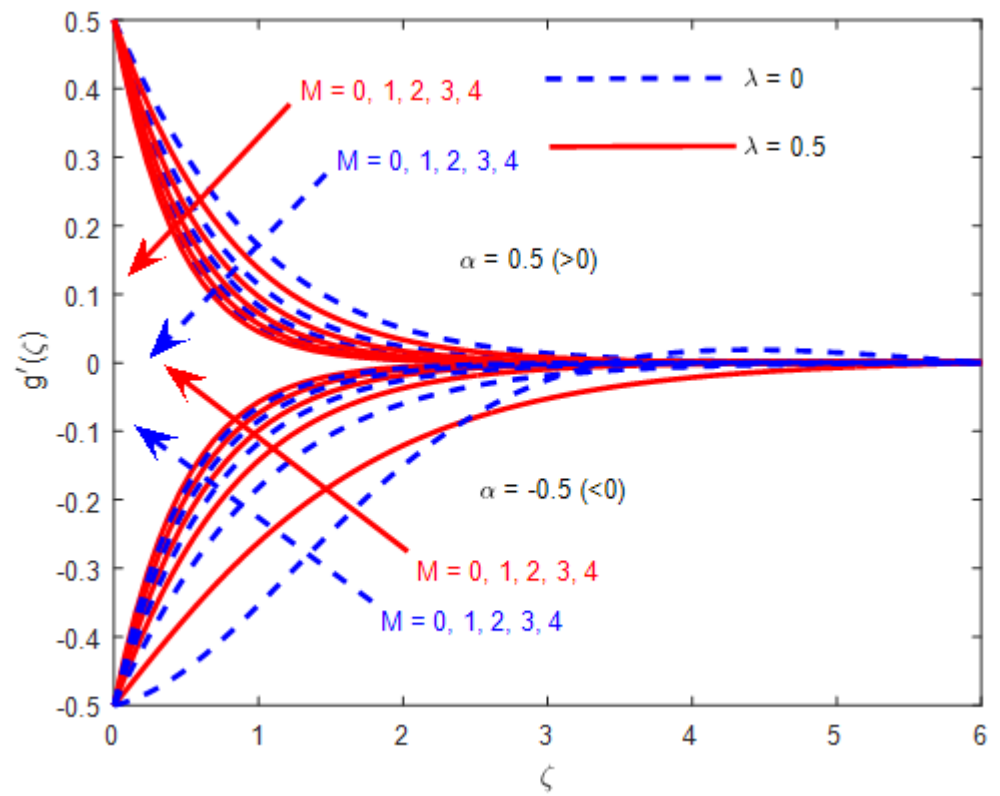


Figure 5. Variation of M and λ on transverse velocity.

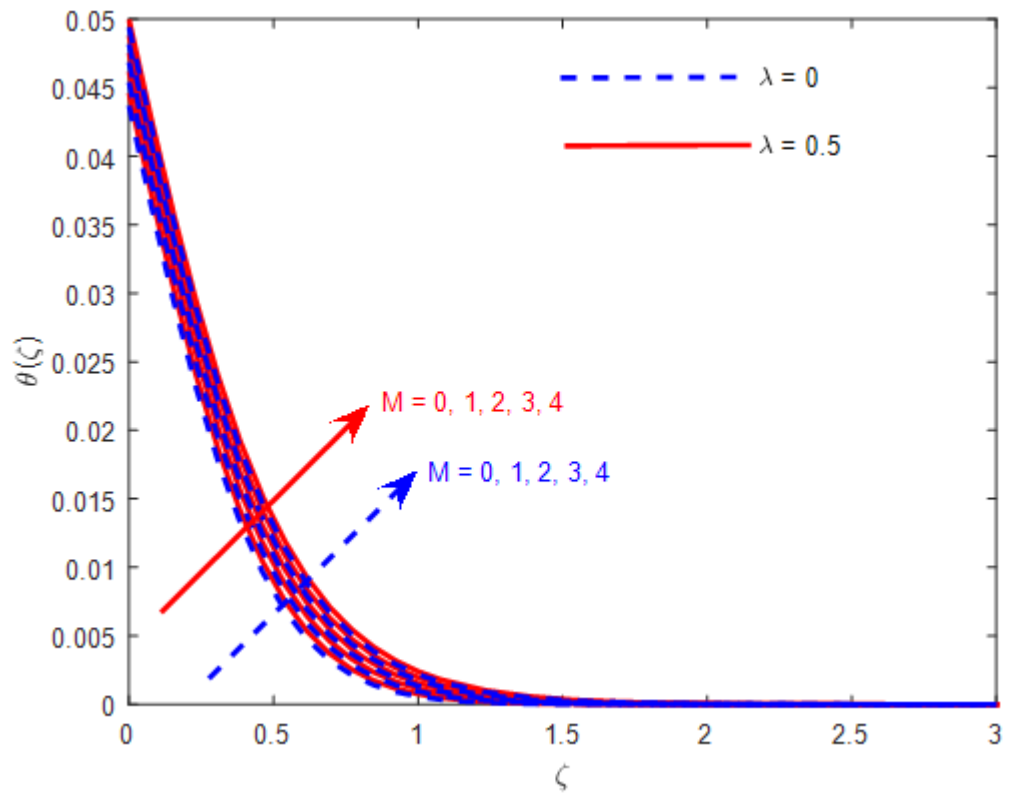


Figure 6. Variation of M and λ on temperature profile.

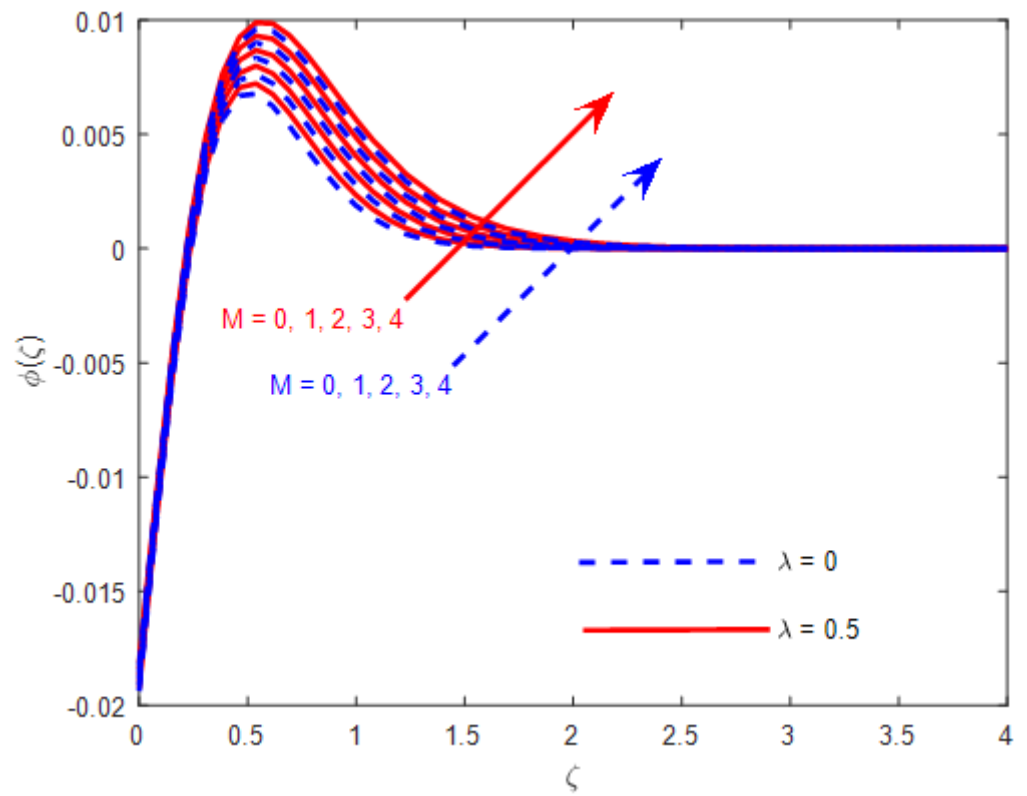


Figure 7. Variation of M and λ on concentration profile.

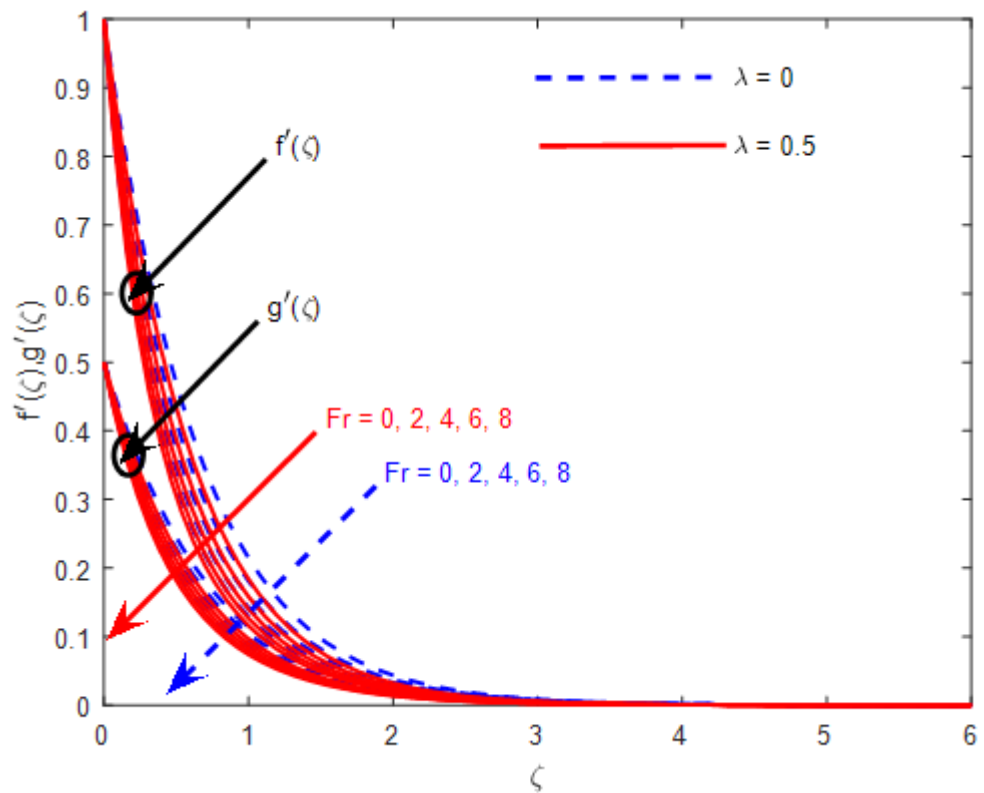


Figure 8. Variation of Fr and λ on axial and transverse velocity.

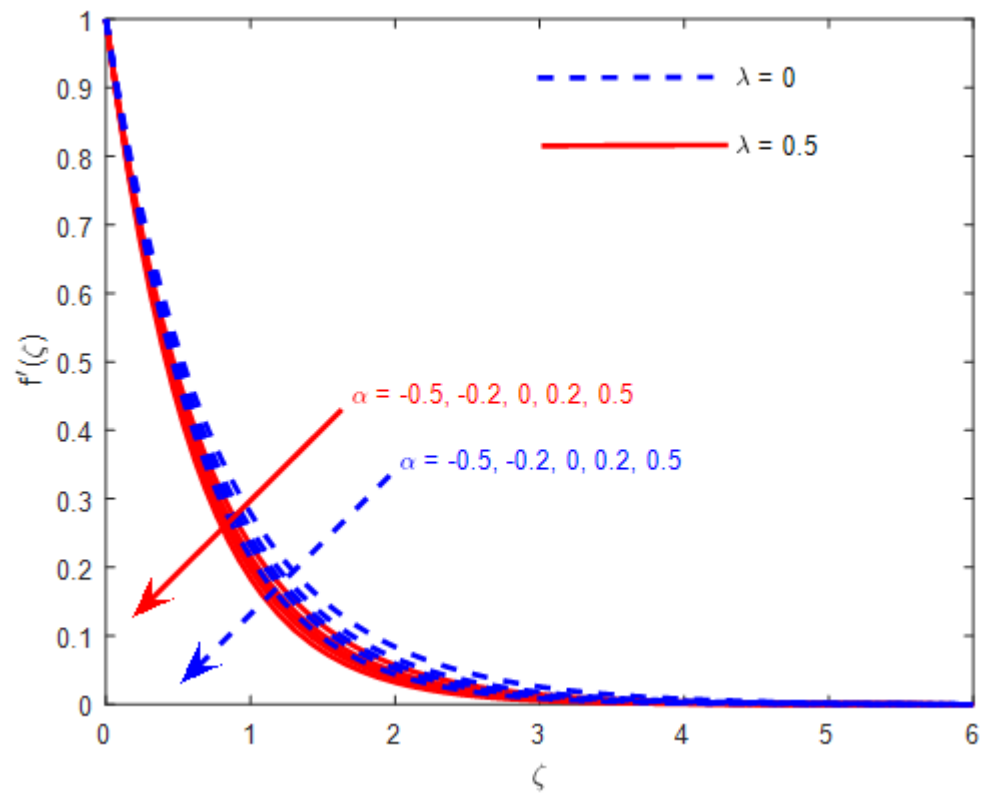


Figure 9. Variation of α and λ on axial velocity.

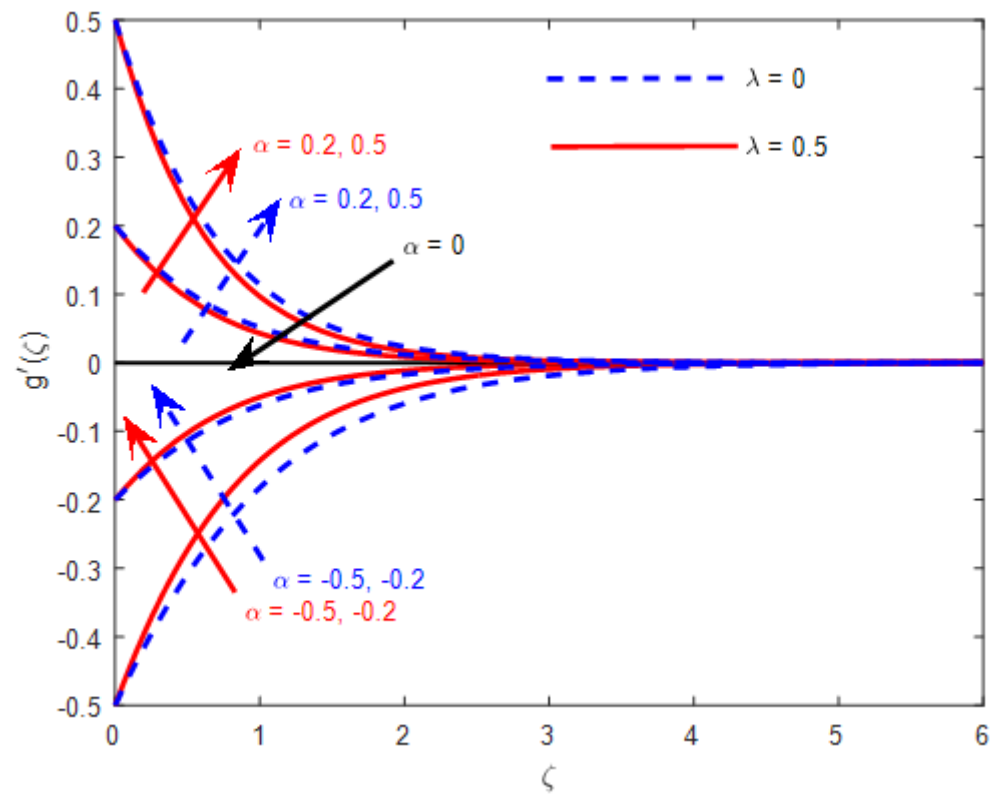


Figure 10. Variation of α and λ on transverse velocity.

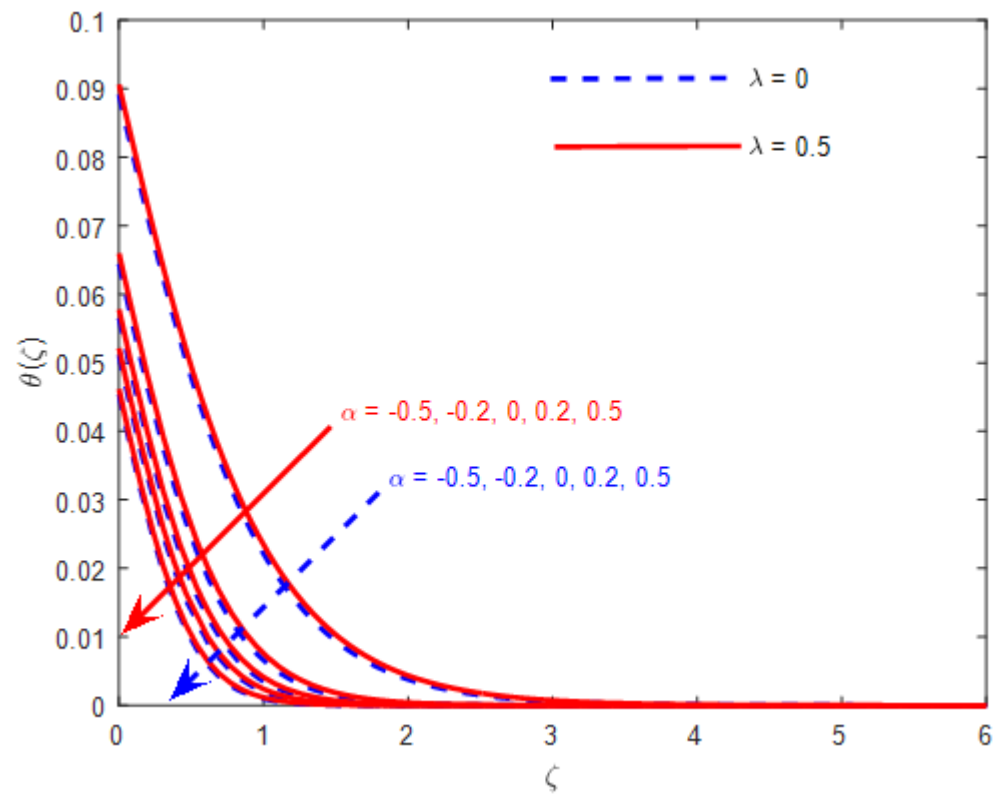


Figure 11. Variation of α and λ on temperature.

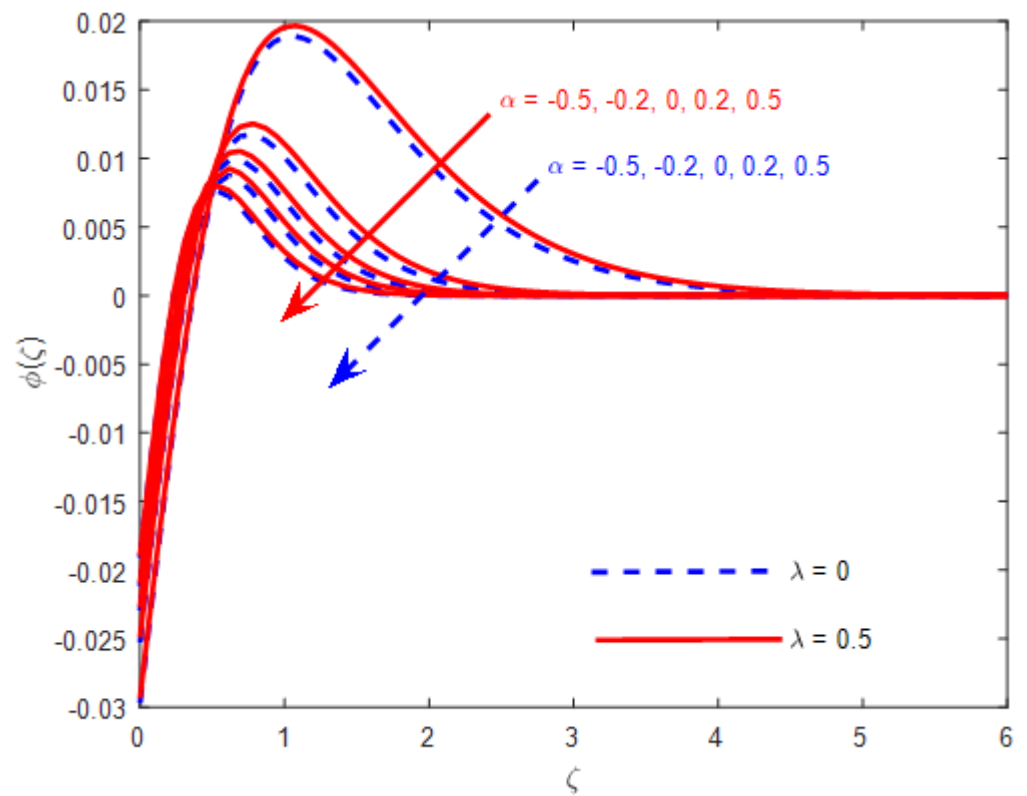


Figure 12. Variation of α and λ on concentration.

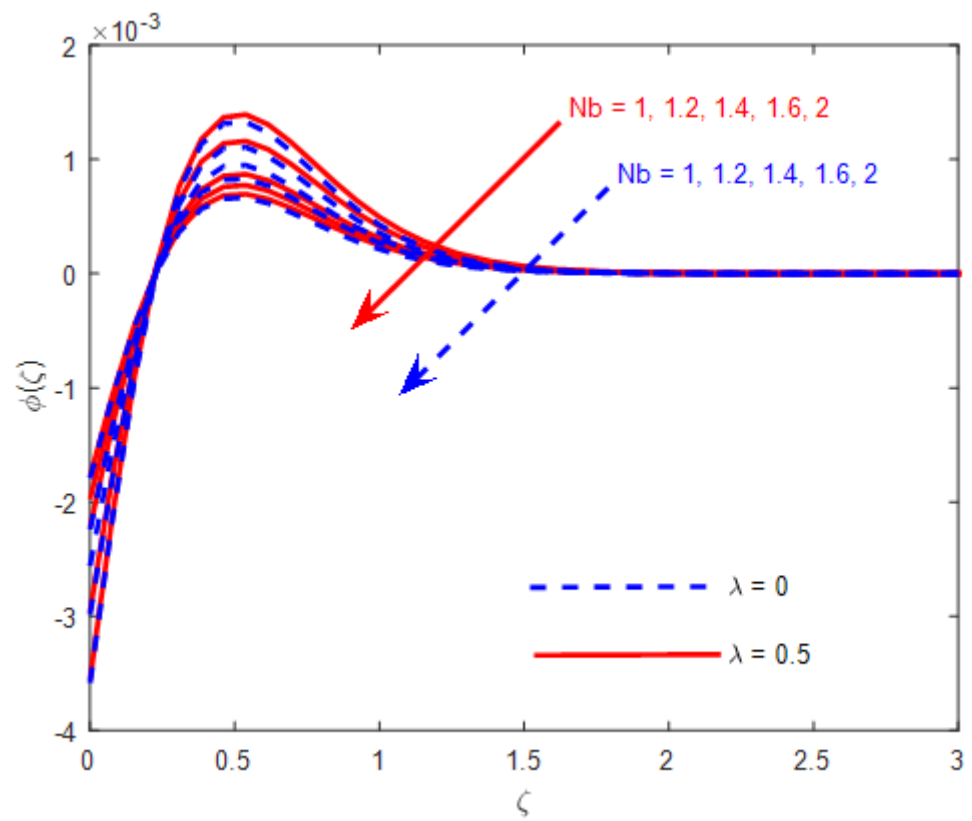


Figure 13. Variation of Nb and λ on concentration.

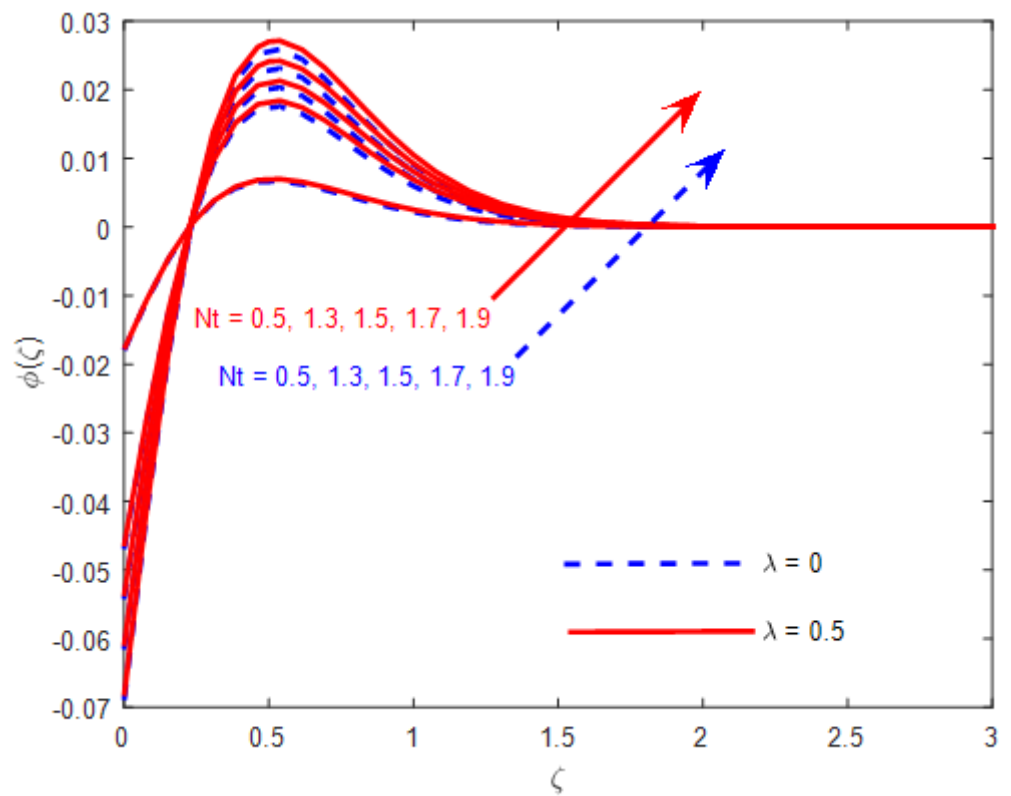


Figure 14. Variation of Nt and λ on concentration.

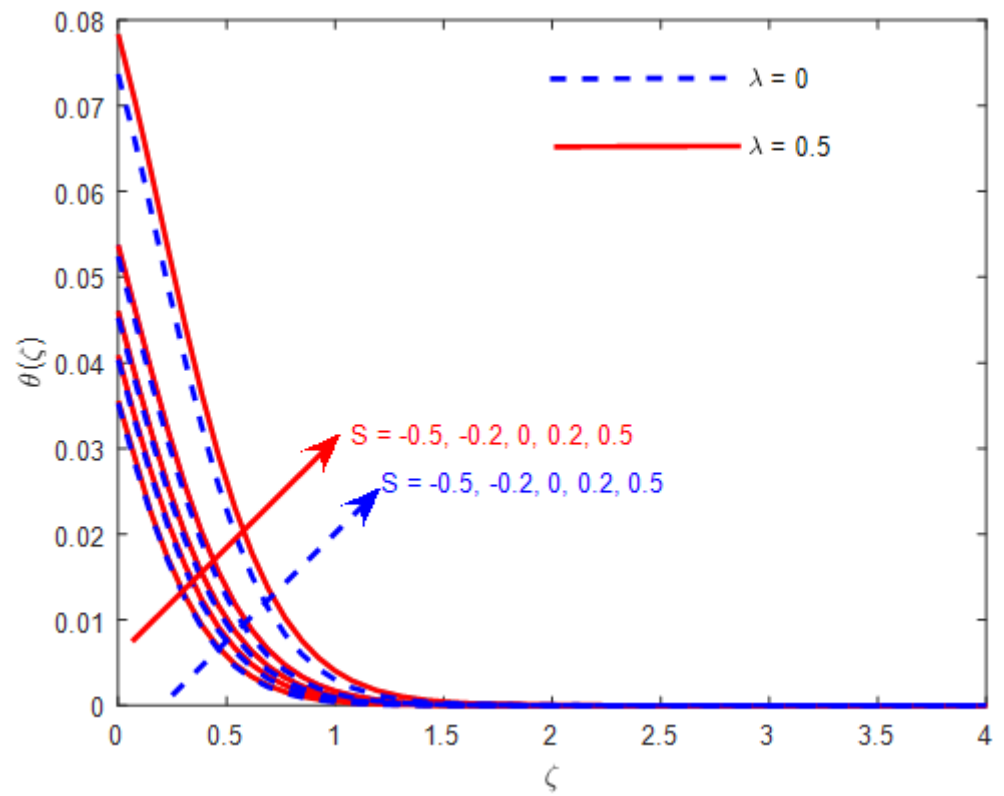


Figure 15. Variation of S and λ on temperature.

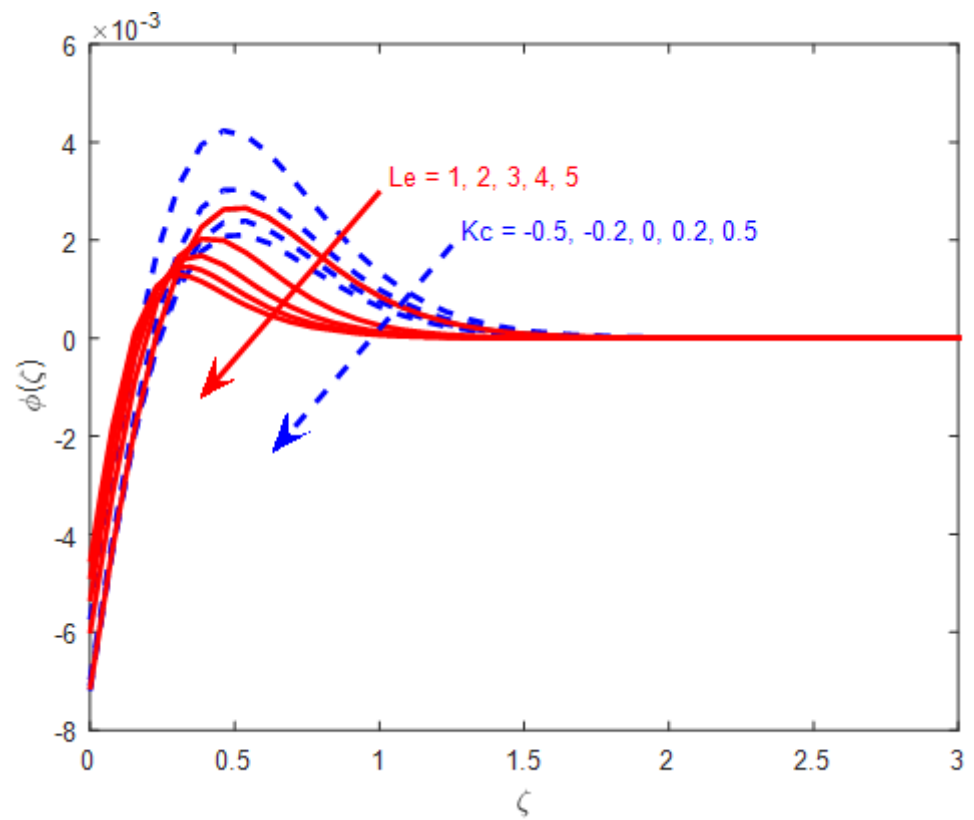


Figure 16. Variation of Le and Kc on concentration.

3.2. Effect of Magnetic Parameter

The applied transverse magnetic field causes the fluid to become magnetized and the impact is due to the force that is created by the magnetic dipole as well as the movement of electric charges. This impact also termed as an electromagnetic effect and it exerts a force near the moving charges and magnetic dipole. Figure 4 illustrates the characteristic of the magnetic constraint affecting the axial velocity profile for the occurrence of a permeable/impermeable medium. Here, in each description $\lambda = 0$ (dotted line) indicates the clear fluid region and $\lambda = 0.5$ (bold lines) presents the flow via a permeable medium. The interaction of the magnetic field gives rise to produce a resistive force in terms of Lorentz force, which renders an opposing or resistive force for which the velocity decelerates regardless of whether the medium is porous or the flow is through a clear fluid domain. This exhibits a strong retardation in surface thickness, which results in the velocity attenuating asymptotically. The analysis of the magnetic effect indicates that the non-magnetized fluid has a more significant impact on enhancing fluid velocity compared to the magnetized fluid. This suggests that the application of a magnetic field plays a crucial role in industrial production processes. Furthermore, the introduction of a porous matrix reduces fluid velocity to a greater extent compared to the flow through a clear fluid domain. Figure 5 illustrates the impression of magnetization on the transverse velocity distribution in various situations of the velocity ratio parameter (α). The study also comprises the impact of porosity on the flow profiles. Here, $\alpha > 0$ suggests the expanding surface and $\alpha < 0$ indicates the contracting surface. When the sheet is stretched, it remains entirely within the positive domain. However, in the case of contraction, it occurs within the negative domain. This indicates that in both scenarios, the thickness of the flow profile decreases towards the bounding surface, which hinders the transverse flow velocity. The permeability of the medium also follows a similar pattern in influencing the velocity distribution. Figure 6 illustrates the combining property of magnetization with a porous matrix on the heat transfer profile. The retarding effect of both the parameters on the velocity distribution reveals that the energy is stored near the surface region and this exerts a greater upsurge in the heat transport phenomenon; therefore, the stored energy gives up and the fluid temperature increases significantly. Although the variation due to a porous matrix is insignificant in a close observation, it is seen that the permeability of the medium renders the maximum temperature within the domain. Figure 7 illustrates how the magnetic parameter changes across the distribution of nanofluid concentrations. A sharp increase in the profile is evident until the point where $\zeta = 0.5$, after which the profile gradually levels off. With increasing magnetic parameter values, the profile consistently improves across the entire range.

3.3. Effect of Inertial Drag

Figure 8 portrays the role of Darcy–Forchheimer inertial drag on the axial as well as transverse fluid velocity distribution with the interaction of a porous matrix. To describe the micro-structural behavior in the pore fluid flow, this drag effect is considered. As discussed earlier, the application of inertial drag is important in mechanical studies; for example, contemplate situations involving hydraulic fracturing, where a fracking fluid is injected into a porous rock to initiate a fracture. In such instances, a Darcy-like pore fluid behavior arises within the porous matrix, transitioning to a Navier–Stokes-type flow at the surface [35]. It reveals that enhanced drag controls the fluid velocity; therefore, in both cases it decelerates smoothly. Further, the presence of a porous matrix enhancing the amount of retardation is greater in comparison to the flow through a clear fluid.

3.4. Effect of Velocity Ratio

Figure 9 describes the velocity ratio on the Darcy–Forchheimer flow of nanofluid velocity distribution due to the impact of a porous matrix. The observation takes a significant attenuation in the velocity distribution for the increasing positive velocity ratio parameter whereas the impact is reversed for the negative values. Figure 10 exhibits the characteristic of the velocity ratio on the transverse velocity profile in combination with the impact of

permeability. Three distinct layers of variations are presented for the various values of the velocity ratio parameter. An interesting feature is exhibited for $\alpha = 0$, i.e., the profile became linear over the main flow direction. Further, the profile augments for the increasing values of the ratio parameter. The variation of positive values is exhibited in the positive domain and the negative values presented in the negative domain. In either of the cases, the flow through an impermeable medium exhibited maximum velocity in magnitude in comparison to a permeable medium. Figures 11 and 12 illustrate the noteworthy traits of the ratio parameter on the temperature and concentration distributions of the nanofluid, respectively. In Figure 11, there is a gradual attenuation in the profile as the positive ratio parameter increases, while the negative ratio parameter intensifies this effect. Moving on to Figure 12, the impact of the ratio parameter on the concentration distribution is displayed. A marked augmentation in the profile is evident within a specific range, followed by a deceleration. Furthermore, an increase in the ratio parameter once again leads to a retarding effect on the concentration profile, regardless of the medium being considered.

3.5. Effect of Brownian and Thermophoresis

Recent studies in biomedical research conforms the usefulness of the Brownian motion for the transport of chemicals and enzymes into the cells of the human body. The effect of Brownian motion occurs due to the existence of the terms $Nb\phi'\theta'$ in Equation (10) and $Nt/Nb\theta''$ in Equation (11). The random motion of the particles in collision with respect to the surrounding gaseous molecules performs the characteristic of the Brownian motion. Figure 13 characterizes the impact of Brownian motion on the solutal concentration profile and the observation shows a dual behavior within the domain for several values. For $\zeta < 0.25$, it is seen that the increasing Brownian motion parameter upsurges the profile and from the point of contact between the profiles, its reverse impact is shown. Further, Figure 14 elaborates the property of thermophoresis on the concentration profile. The appearance of $Nt\theta'^2$ is in Equation (10) and $Nt/Nb\theta''$ in Equation (11). It occurs due to the combined impact of the temperature gradient in the concentration distribution. However, the profile enhances for the increasing values of the thermophoresis parameter irrespective of the permeability.

3.6. Effect of Heat Source/Sink

Figure 15 exhibits the impact of additional heat source/sink on the fluid temperature distribution that enhances the profile in conjunction with the convective boundary condition due to the flow through a permeable/impermeable medium. Here, $S > 0$ presents the behavior of source and $S < 0$ indicates the role of sink that affects the heat transport phenomenon. Further, the absence of heat source/sink is also exhibited in the corresponding figure. Increasing heat source exhibits the smooth enhancement in the fluid temperature whereas the opposite impact is rendered for the role of sink.

3.7. Effect of Lewis Number and Chemical Reaction

Figure 16 exhibits the impact of Lewis number as well as the chemical reaction parameter on the solutal profiles of nanofluid. The Lewis number is the combined effect of the heavier species and the Prandtl number. Mathematically, the Lewis number is the ratio of the thermal diffusivity and the Brownian diffusivity. Increasing the Lewis number is due to deceleration in the Brownian diffusivity; therefore, the concentration profile retards significantly. Here, $Kc > 0$ presents the destructive chemical reaction, $Kc < 0$ indicates the constructive, and $Kc = 0$ suggests the no chemical reaction that validates the earlier study. The observation reveals that the increasing destructive chemical reaction retards the solutal profile while the constructive shows a reverse impact on the concentration profile.

4. Conclusions

A numerical treatment on the flow of Darcy–Forchheimer model nanofluid over an expanding surface is analyzed in the present investigation. The convective heat and solutal

boundary condition enriches the flow phenomena significantly. The behavior of several physical quantities on the various profiles are exhibited and described briefly. Further, the important characteristics are:

- Thorough examination reveals a strong alignment between the present numerical findings and those of a prior investigation, indicating a notable correlation. Furthermore, it affirms the adherence of the current methodology to the convergence criteria. This analysis paves the way for future advancements in research along this trajectory.
- The streamlines for the proposed stream function shows the flow pattern of the fluid particles within the domain for the variation of the kinematic viscosity and stream values. The increasing values show a greater sharpness away from the stagnation point.
- Magnetized fluid for the interaction of the resistive forces such as the electromagnetic field and the porous matrix resists the fluid axial and transverse velocity whereas the enhancement is quite adequate in the fluid temperature, and the concentration is exhibited.
- The enhanced Brownian motion controls the fluid concentration for the absence/presence of permeability but the thermophoresis parameter encourages it.
- The heavier species representing the Lewis number along with the reacting agents favorable for diminishing the fluid concentration at all points within the domain.

Author Contributions: Conceptualization, P.C.P. and S.R.M.; methodology, S.J.; software, M.A.; validation, S.R.M. and N.A.S.; formal analysis, P.C.P.; investigation, S.J.; resources, M.A.; data curation, N.A.S.; writing—original draft preparation, P.C.P. and S.J.; writing—review and editing, M.A. and N.A.S.; supervision, S.R.M.; All authors have read and agreed to the published version of the manuscript.

Funding: This project was supported by the Researchers Supporting Project number (RSP2023R411), King Saud University, Riyadh, Saudi Arabia.

Data Availability Statement: The data that support the findings of this paper are available from the corresponding author upon reasonable request.

Acknowledgments: This project was supported by the Researchers Supporting Project number (RSP2023R411), King Saud University, Riyadh, Saudi Arabia.

Conflicts of Interest: The authors declare no conflict of interest.

Nomenclature

Roman

u, v, w	Momentum components along coordinate axes (x, y, z)
u_w	Plate velocity [M/S]
v_w	Suction velocity [M/S]
T	Fluid temperature [K]
T_w	Plate temperature [K]
T_∞	Ambient temperature attained [K]
C_∞	Ambient concentration
B_0	Magnetic strength
h_f, T_f	Heat transport coefficient
C_b	Amount of drag
D_B	Brownian diffusion (m^2/s)
D_T	Thermophoretic diffusion (m^2/s)
F	Drag coefficient
K	Permeability (m^2)
k	Thermal conductivity

M	Magnetic parameter
Fr	Darcy–Forchheimer parameter
Kc	Reactive species
Le	Lewis number
Pr	Prandtl number
Sc	Schmidt number
Nt	Thermophoresis parameter
Nb	Brownian motion
S	Heat source/sink
$f(\eta)$	Dimensionless stream function
<i>Greek symbols</i>	
ψ	Stream function
ν	Kinematic viscosity (m ² /s)
μ	Dynamic viscosity (m ² /s)
α_m	Thermal diffusivity (m ² /s)
λ	Porosity parameter
γ	Biot Number
τ	Heat capacity ratio $\frac{(\rho c)_p}{(\rho c)_f}$
ρ	Fluid density (Kg/m ³)
$(\rho c)_p$	Heat capacity of the solid particle
$(\rho c)_f$	Heat capacity of the fluid
ρ_p	Particle density [kg/m ³]
<i>Subscripts</i>	
w	Sheet condition

References

- Choi, S.U.S.; Eastman, J.A. Enhancing Thermal Conductivity of Fluids with Nanoparticles. In Proceedings of the 1995 International Mechanical Engineering Congress and Exhibition, San Francisco, CA, USA, 12–17 November 1995; pp. 99–105.
- Choi, S.U.S.; Zhang, Z.G.; Yu, W.; Lockwood, F.E.; Grulke, E.A. Anomalous thermal conductivity enhancement in nanotube suspensions. *Appl. Phys. Lett.* **2001**, *79*, 2252–2254. [[CrossRef](#)]
- Eastman, J.A.; Choi, U.S.; Li, S.; Thompson, L.J.; Lee, S. Enhanced Thermal Conductivity through the Development of Nanofluids. In Proceedings of the 996 Fall meeting of the Materials Research Society (MRS), Boston, MA, USA, 2–6 December 1996; Volume 457, pp. 3–11. [[CrossRef](#)]
- Wang, X.-Q.; Mujumdar, A.S. Heat transfer characteristics of nanofluids: A review. *Int. J. Therm. Sci.* **2007**, *46*, 1–19. [[CrossRef](#)]
- Eastman, J.; Phillpot, S.; Choi, S.; Keblinski, P. Thermal transport in nanofluids. *Annu. Rev. Mater. Res.* **2004**, *34*, 219–246. [[CrossRef](#)]
- Kakac, S.; Pramuanjaroenki, A. Review of convective heat transfer enhancement with nanofluids. *Int. J. Heat Mass Transf.* **2009**, *52*, 3187–3196. [[CrossRef](#)]
- Wang, C.Y. Fluid flow due to a stretching cylinder. *Phys. Fluids* **1988**, *31*, 466–468. [[CrossRef](#)]
- Fang, T.; Yao, S. Viscous Swirling Flow over a Stretching Cylinder. *Chin. Phys. Lett.* **2011**, *28*, 114702. [[CrossRef](#)]
- Chandini Pattanaik, P.; Mishra, S.R.; Jena, S.; Pattnaik, P.K. Impact of radiative and dissipative heat on the Williamson nanofluid flow within a parallel channel due to thermal buoyancy. *J. Nanomater. Nanoeng. Nanosyst.* **2022**, *236*, 3–18.
- Naseer, M.; Malik, M.Y.; Nadeem, S.; Rehman, A. The boundary layer flow of hyperbolic tangent fluid over a vertical exponentially stretching cylinder. *Alex. Eng. J.* **2014**, *53*, 747–750. [[CrossRef](#)]
- Majeed, A.; Javed, T.; Ghaffari, A.; Rashdi, M.M. Analysis of heat transfer due to stretching cylinder with partial slip and pre-scribed heat flux. *Alex. Eng. J.* **2015**, *54*, 1029–1036. [[CrossRef](#)]
- Shojaei, A.; Amiri, A.J.; Ardahaie, S.S.; Hosseinzadeh, K.; Ganji, D. Hydrothermal analysis of Non-Newtonian second grade fluid flow on radiative stretching cylinder with Soret and Dufour effects. *Case Stud. Therm. Eng.* **2018**, *13*, 100384. [[CrossRef](#)]
- Zhou, W.N.; Yan, Y.Y. Numerical Investigation of the Effects of a Magnetic Field on Nanofluid Flow and Heat Transfer by the Lattice Boltzmann Method. *Numer. Heat Transf. Part A Appl.* **2015**, *68*, 1–16. [[CrossRef](#)]
- Ashorynejad, H.R.; Sheikholeslami, M.; Pop, I.; Ganji, D.D. Nanofluid flow and heat transfer due to a stretching cylinder in the presence of magnetic field. *Heat Mass Transf.* **2013**, *49*, 427–436. [[CrossRef](#)]
- Mukhopadhyay, S.; Ishak, A. Mixed Convection Flow along a Stretching Cylinder in a Thermally Stratified Medium. *J. Appl. Math.* **2012**, *2012*, 491695. [[CrossRef](#)]
- Tlili, I. Effects MHD and Heat Generation on Mixed Convection Flow of Jeffrey Fluid in Microgravity Environment over an Inclined Stretching Sheet. *Symmetry* **2019**, *11*, 438. [[CrossRef](#)]

17. Javaherdeh, K.; Nejad, M.M.; Moslemi, M. Natural convection heat and mass transfer in MHD fluid flow past a moving vertical plate with variable surface temperature and concentration in a porous medium. *Eng. Sci. Technol. Int. J.* **2015**, *18*, 423–431. [[CrossRef](#)]
18. Raju, C.; Sandeep, N.; Saleem, S. Effects of induced magnetic field and homogeneous–heterogeneous reactions on stagnation flow of a Casson fluid. *Eng. Sci. Technol. Int. J.* **2016**, *19*, 875–887. [[CrossRef](#)]
19. Sheikholeslami, M. Numerical investigation for CuO-H₂O nanofluid flow in a porous channel with magnetic field using mesoscopic method. *J. Mol. Liq.* **2018**, *249*, 739–746. [[CrossRef](#)]
20. Sheikholeslami, M. Numerical simulation of magnetic nanofluid natural convection in porous media. *Phys. Lett. A* **2017**, *381*, 494–503. [[CrossRef](#)]
21. Wakif, A.; Boulahia, Z.; Mishra, S.R.; Rashidi, M.M.; Sehaqui, R. Influence of a uniform transverse magnetic field on the thermo-hydrodynamic stability in water-based nanofluids with metallic nanoparticles using the generalized Buongiorno’s mathematical model. *Eur. Phys. J. Plus* **2018**, *133*, 181. [[CrossRef](#)]
22. Bhatti, M.M.; Mishra, S.R.; Abbas, T.; Rashidi, M.M. A mathematical model of MHD nanofluid flow having gyrotactic microorganisms with thermal radiation and chemical reaction effects. *Neural Comput. Appl.* **2016**, *30*, 1237–1249. [[CrossRef](#)]
23. Siddiqui, A.; Azim, Q. Creeping flow of a viscous fluid in a uniformly porous slit with porous medium: An application to the diseased renal tubules. *Chin. J. Phys.* **2020**, *64*, 264–277. [[CrossRef](#)]
24. Hayat, T.; Aziz, A.; Muhammad, T.; Alsaedi, A. Darcy–Forchheimer Three-Dimensional Flow of Williamson Nanofluid over a Convectively Heated Nonlinear Stretching Surface. *Commun. Theor. Phys.* **2017**, *68*, 387. [[CrossRef](#)]
25. Muhammad, T.; Alsaedi, A.; Hayat, T.; Shehzad, S.A. A revised model for Darcy–Forchheimer three-dimensional flow of nanofluid subject to convective boundary condition. *Results Phys.* **2017**, *7*, 2791–2797. [[CrossRef](#)]
26. Acharya, S.; Nayak, B.; Mishra, S.R.; Jena, S. Adomian decomposition method for the MHD flow of a viscous fluid with the influence of dissipative heat energy. *Heat Transf.* **2020**, *49*, 4612–4625. [[CrossRef](#)]
27. Pattnaik, P.K.; Mishra, S.; Jena, S. Dissipative heat for the Casson fluid flow past an expanding cylindrical surface. *Heat Transf.* **2022**, *51*, 2476–2487. [[CrossRef](#)]
28. Jena, S.; Mishra, S.R.; Aghaeiboorkheili, M.; Pattnaik, P.K.; Muduli, K. Impact of Newtonian heating on the conducting Casson fluid flow past a stretching cylinder. *J. Interdiscip. Math.* **2022**, *25*, 2401–2416. [[CrossRef](#)]
29. Hayat, T.; Haider, F.; Muhammad, T.; Alsaedi, A. Three-dimensional rotating flow of carbon nanotubes with Darcy–Forchheimer porous medium. *PLoS ONE* **2017**, *7*, e0179576. [[CrossRef](#)]
30. Ramesh, G.K. Darcy–Forchheimer flow of Casson nanofluid with heat source/sink: A three dimensional study. In *Heat and Mass Transfer: Advances in Modelling and Experimental Study for Industrial Applications*; IntechOpen: London, UK, 2018; pp. 43–88.
31. Muskat, M. The Flow of Homogeneous Fluids Through Porous Media. *Soil Sci.* **1938**, *46*, 169. [[CrossRef](#)]
32. Li, Y.-X.; Muhammad, T.; Bilal, M.; Khan, M.A.; Ahmadian, A.; Pansera, B.A. Fractional simulation for Darcy–Forchheimer hybrid nanofluid flow with partial slip over a spinning disk. *Alex. Eng. J.* **2021**, *60*, 4787–4796. [[CrossRef](#)]
33. Rasool, G.; Shafiq, A.; Alqarni, M.S.; Wakif, A.; Khan, I.; Bhutta, M.S. Numerical Scrutinization of Darcy–Forchheimer Relation in Convective Magnetohydrodynamic Nanofluid Flow Bounded by Nonlinear Stretching Surface in the Perspective of Heat and Mass Transfer. *Micromachines* **2021**, *12*, 374. [[CrossRef](#)]
34. Nayak, M.K.; Mabood, F.; Tlili, I.; Dogonchi, A.S.; Khan, W.A. Entropy optimization analysis on nonlinear thermal radiative electromagnetic Darcy–Forchheimer flow of SWCNT/MWCNT nanomaterials. *Appl. Nanosci.* **2021**, *11*, 399–418. [[CrossRef](#)]
35. Atashafrooz, M.; Sajjadi, H.; Delouei, A.A. Simulation of combined convective–radiative heat transfer of hybrid nanofluid flow inside an open trapezoidal enclosure considering the magnetic force impacts. *J. Magn. Magn. Mater.* **2023**, *567*, 170354. [[CrossRef](#)]
36. Atashafrooz, M.; Sajjadi, H.; Delouei, A.A. Interacting influences of Lorentz force and bleeding on the hydrothermal behaviors of nanofluid flow in a trapezoidal recess with the second law of thermodynamics analysis. *Int. Commun. Heat Mass Transf.* **2019**, *110*, 104411. [[CrossRef](#)]
37. Lou, Q.; Ali, B.; Rehman, S.U.; Habib, D.; Abdal, S.; Shah, N.A.; Chung, J.D. Micropolar Dusty Fluid: Coriolis Force Effects on Dynamics of MHD Rotating Fluid When Lorentz Force Is Significant. *Mathematics* **2022**, *10*, 2630. [[CrossRef](#)]
38. Sowmya, G.; Gireesha, B.J.; Animasaun, I.L.; Shah, N.A. Significance of buoyancy and Lorentz forces on water-conveying iron(III) oxide and silver nanoparticles in a rectangular cavity mounted with two heated fins: Heat transfer analysis. *J. Therm. Anal. Calorim.* **2021**, *144*, 2369–2384. [[CrossRef](#)]

Disclaimer/Publisher’s Note: The statements, opinions and data contained in all publications are solely those of the individual author(s) and contributor(s) and not of MDPI and/or the editor(s). MDPI and/or the editor(s) disclaim responsibility for any injury to people or property resulting from any ideas, methods, instructions or products referred to in the content.